Journal of Materials Chemistry C

ROYAL SOCIETY OF CHEMISTRY

PAPER

View Article Online
View Journal | View Issue

Cite this: J. Mater. Chem. C, 2022, 10, 13913

Pre- and post-assembly modifications of colloidal plasmonic arrays: the effect of size distribution, composition and annealing†

Oriol Colomer-Ferrer, ‡ Serni Toda Cosi, ‡ Ylli Conti, David E. Medina-Quiroz, Leonardo Scarabelli * and Agustin Mihi

Templated self-assembly has emerged as one of the most versatile approaches for the fabrication of plasmonic ordered arrays composed of colloidal nanoparticle clusters, representing a valid alternative to top-down lithography for the scalable and low-cost production of this type of plasmonic substrates. Templated self-assembly can be applied to a variety of materials, solvents, and colloidal size, shape, and composition. A higher degree of control over the preparation of the colloids and their assembly would enable the rational modification of the internal composition and architecture of the repeating units of the array, targeting specific properties and applications. In this work, we explored both pre- and post-assembly modifications of the plasmonic system, analyzing their effect on the resulting collective optical properties. Combining both gold nanoparticles of different sizes and mixtures of gold and silver colloids, we demonstrated the possibility of leveraging near- and far-field coupling to control the optical losses of the system. Moreover, we explored the application of a thermal annealing step to induce the sintering of the colloidal building blocks within the plasmonic clusters. At lower temperatures (300 °C), the resulting single plasmonic objects are characterized by an inhomogeneous elemental distribution, while atomic migration and formation of alloys is triggered at higher temperatures (450 °C). By systematically analyzing the effect of the annealing we show an improvement in lattice plasmonic resonance quality factor of a gold nanoparticle array by 20%, without compromising its characteristic chemical and physical stability. Collectively, our results establish intriguing directions for the preparation of plasmonic arrays where the repeating unit can be engineered either before or after the assembly targeting specific catalytic, optical or magnetic properties.

Received 21st March 2022,
Accepted 15th June 2022

DOI: 10.1039/d2tc01148d

rsc.li/materials-c

1. Introduction

Localized surface plasmon resonances (LSPRs), the coherent oscillations of conductive electrons in response to an impinging electromagnetic wave, have found potential application in several scientific areas, exploiting their extremely high absorption cross-sections, the consequent enhancement of electric and magnetic fields, and the several possible relaxation pathways of the excited electrons.[1–3] However, LSPRs in metal nanoparticles

Institute of Materials Science of Barcelona (ICMAB-CSIC), Campus de la UAB, 08193 Bellaterra, Catalonia, Spain. E-mail: lscarabelli@icmab.es

† Electronic supplementary information (ESI) available: Materials and experimental details for the synthesis and preparation of the different colloids and the self-assembly process. Information and instrumentation setup description for spectroscopic and electron microscopy characterization of the substrates. Full characterization of the colloids and colloidal mixtures, additional scanning electron microscopy images, illumination angle dependency of the transmittance profiles. See DOI: https://doi.org/10.1039/d2tc01148d

‡ These authors contributed equally to this work.

Leonardo Scarabelli

Leonardo Scarabelli earned his BSc and MSc in chemistry from the University of Pavia, and received his PhD from the University of Vigo in 2016, under the direction of Prof. L. M. Liz-Marzán. After training as a postdoc at the University of California, Los Angeles, in the laboratory of Prof. P. S. Weiss, he began his independent academic career at the Institute of Materials Science of Barcelona (ICMAB) as a "La Caixa" Junior Leader. His current interests include the development of unconventional strategies for the direct surface synthesis of plasmonic arrays, and their implementation into strong-coupled hybrid plasmonic materials.

are also characterized by inherently high optical losses,[4,5] reducing the lifetimes of the resonances and posing severe limitations for applications such as catalysis, optoelectronic and communication devices.

Plasmonic ordered arrays represent a convenient way to overcome these limitations. In this configuration, the diffractive states of the array (defined by Bragg conditions) are able to mediate the far-field coupling between the repeating units.[6] This leads to the coupling between the LSPRs of the repeating units and the diffraction modes of the array at the Rayleigh–Wood anomalies,[7,8] generating lattice plasmonic resonances (LPRs) characterized by a wide spectral tunability, highly delocalized energy states and narrow bandwidth.[4,9–11]

While top-down fabrication approaches such as electron beam lithography and metal evaporation have been used for the early study of these types of substrates, more affordable and easily-scalable approaches have recently emerged, combining soft-lithography and self-assembly of pre-synthetized plasmonic colloids.[12]

For example, self-assembly of various colloids was demonstrated by both dip and spin coating,[13] while capillary- and DNA-assisted self-assembly enabled single-particle organization at the nanoscale by optimization of template topography.[14,15] Another technique that emerged recently is electrophoretic self-assembly, where charged colloids are precisely organized on electrically conductive surfaces.[16] This technique demonstrated a higher degree of control over nanoparticles orientation in the final assembly, an important step forward for controlling polarization-dependent effects,[17] and bridge the gap with top-down fabrication. However, all these techniques require the dissolution of the template or the transfer of the particles to the desired substrate.[18] On the contrary, in templated self-assembly a pre-patterned elastomeric mold is used to induce ordering of the nanoparticles directly on top of the substrate of choice. The organization of the colloid is driven by solvent evaporation at the edges of the wetted area, resulting in the self-assembly of the nanoparticles into superstructures with size and shape of the template cavities. The conditions for the self-assembly are optimized to ensure a homogeneous distribution of the colloid over the substrate, and an accurate reproduction of the template morphology.[19] This approach is one of the most versatile self-assembly techniques, being compatible with different colloids (varying shape/size/composition/surface chemistry), materials, and solvents.[19,20] Moreover, the production of multiple elastomeric replicas of the original master dramatically reduces the impact of the its fabrication cost, which can be realized by standard lithographic technique such as electron-beam lithography, or with more cost-effective approaches such as nanosphere lithography.[21]

The versatility of templated self-assembly has been exploited for the fabrication of complex functional devices, such as mechano-tunable plasmonic devices,[22] chirally active substrates,[23] and multicomponent architectures for plasmon-enhanced up-conversion luminescence.[24] Moreover, several applications have been targeted using templated self-assembled structures, including surface-enhanced Raman scattering,[25,26] tumor monitoring,[27] and catalysis.[28]

An interesting direction that remained relatively unexplored by the community is the possibility to modify optical properties of the plasmonic arrays acting on the internal structure of the repeating unit. This perspective is especially interesting for colloidal assemblies, as these modifications can potentially be pre-designed into the colloidal building-blocks used for the assembly, exploiting directional surface chemistry, specific interaction with the substrates, as well as crystallinity or chemical reactivity.[11,29]

In this direction, we recently demonstrated the dramatic influence of controlling the optical losses of the system on the quality factor of the lattice plasmon resonances of gold nanoparticle clusters array, and we were able to achieve very narrow plasmon resonances (quality factor, $Q_F > 60$) by simply optimizing nanoparticle sizes.[30]

Herein, we expand these concepts and explore both pre- and post-assembly modification of the repeating unit, analyzing their effects on the collective plasmonic response. Specifically, we first used a co-assembly strategy to prepare plasmonic arrays composed of colloids of different sizes and compositions. Finally, we explored a thermal post-modification of the prepared structures; this treatment enables the preparation of heterogeneous agglomerates and alloying of the original components, depending on the temperature and dwelling time. The generalization of the proposed strategies could lead to the preparation of plasmonic materials for biosensing, photocatalysis, or efficient light manipulation.

2. Results and discussion

Plasmonic arrays are fabricated *via* templated self-assembly of pre-synthetized colloids (Fig. 1), following a procedure reported previously.[30] Briefly, colloidal nanoparticles with a narrow size dispersion (<15%, Fig. S1, ESI†) are synthetized by colloidal growth,[30,31] functionalized with a thiol-terminated polyethyleneglycol (PEG-SH, M_W = 2000) and concentrated (see Experimental section) in a water : ethanol 60 : 40 mixture in the presence of a small concentration of cationic surfactant (cetyltrimethylammonium chloride, or CTAC, 50 μM). These conditions were selected to control the organization of the colloids during the assembly, avoiding coffee ring and Marangoni effects, ensuring the preferential adhesion of the nanoparticles to the substrate, and a homogeneous coverage.[19] To induce the self-assembly of the colloids into plasmonic arrays, a 1 μL aliquot of the selected colloidal suspension is drop-casted over a hydrophilic surface, and immediately covered by a polydimethyl siloxane (PDMS) mold patterned with a square array of cavities that confined the particles during the evaporation of the solvent. Since the manuscript is focused on the modification of the repeating unit, the geometrical parameters of the PDMS mold have been kept constant throughout the work, consisting of a square array of 500 nm in pitch, with a hole size of 280 nm in diameter. Templated self-assembly can easily

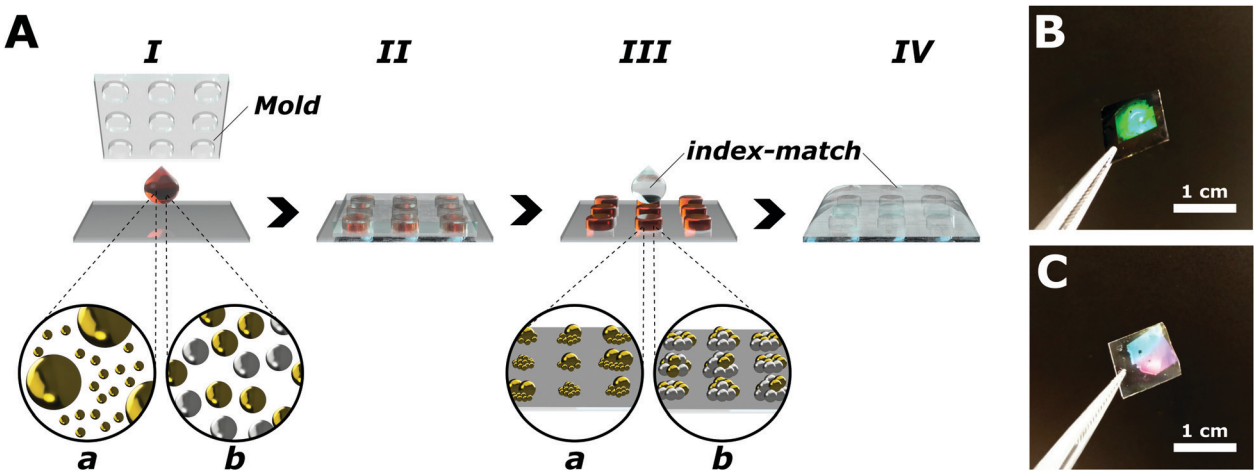

Fig. 1 Self-assembly of plasmonic arrays. (A) Schematic illustration of the fabrication process of two-dimensional plasmonic arrays. I: drop-cast of the colloidal mixture and application of the mold; II: self-assembly of the colloid into confined space driven by solvent evaporation; III: results of the demolding, yielding plasmonic arrays made of the corresponding colloidal suspension; IV: application of the index-matching layer. (a) Gold colloid of different sizes. (b) Gold and silver colloids. (B) and (C) Pictures of a typical large-scale substrate after preparation on glass (B) and silicon (C), before index-matching.

target a wide variety of lattice parameters and array geometries (*e.g.* hexagonal, rectangular, or honeycomb), enabling the extension of our results to more complex architectures and optical responses. The nominal depth of the holes in the template is 390 nm; however, the final height of the clusters composing the array is controlled by the concentration of the colloid used for the assembly, following an hcp organization of the nanoparticles within each cluster.[32] The area of the obtained plasmonic array is limited by the original master dimension to an area of 49 mm^2, but templated self-assembly compatibility with a roll-to-roll setup ensure the possibility to easily scale-up our fabrication approach. The prepared plasmonic arrays are mechanically and chemically stable for several days at room temperature. Before proceeding to optical characterization, a layer of PDMS (>100 μm) was applied on top of the plasmonic units to ensure a uniform dielectric environment (n = 1.45, see Experimental section). This superstrate maximizes the in-plane coupling mediated by the grazing diffraction modes, facilitating the emergence and the study of the lattice resonances.[33–35]

The optical response of the colloidal plasmonic crystals can be described to a first approximation by two spectral features: the LSPR of the plasmonic clusters appearing between 400 and 650 nm, and the collective response of the array as a whole. The position of the LPRs can be predicted using a simplified equation deriving from Bragg conditions.[19,30] In the specific case of a square array investigated under normal illumination incidence with scramble polarized light, the spectral position of the first diffraction order corresponding to the lowest energy LSP can be predicted by:

$$\lambda_{LPR} = \Lambda \cdot n_{eff} \quad (1)$$

where Λ is the lattice parameter of the grating, and n_{eff} is the effective refractive index of the surrounding dielectric media. For this manuscript, Λ = 500 nm and n_{eff} = 1.49 (considering an average of both n_{glass} = 1.52 and n_{PDMS} = 1.45) are constant for all the samples, predicting the position of the main LPR around 745 nm.

2.1 Pre-assembly modifications: the effect of colloid size dispersity

In the first study, gold nanoparticles of two different sizes (96 ± 9 and 24 ± 3 nm, see Fig. S1, ESI†) were assembled into 500 nm square arrays. The colloidal suspensions were brought at the same gold concentration ($[Au^0]$ = 50 mM) using the absorbance of the gold interband transition at 400 nm.[36] Subsequently, two different mixtures were prepared using a 1 : 1 and a 1 : 3 volume ratio between 25 and 100 nm colloids. The resulting plasmonic arrays were compared with the assemblies of the single components. As can be observed in the scanning electron microscopy (SEM) analysis (Fig. 2(A)–(D)), the presence of the two colloidal populations did not disrupt the self-assembly process, yielding large-scale organization into plasmonic arrays. Moreover, despite the significant volume difference (64 times), both small and bigger colloids were co-assembled within the same cluster structures. However, in the 1 : 1 ratio case, several clusters were solely composed of 25 nm colloids (Fig. 2(B)). This can be explained by the different translational diffusion coefficient, which is linked to the colloid diameter by the Stokes–Einstein equation, indicating that the 25 nm colloid would immediately start filling the cavities of the mold, preventing the bigger 100 nm gold particles to occupy the same space.

Different size combinations were tested by changing either the bigger or the smaller colloids for 49 ± 3 nm gold nanoparticles. A higher percentage of clusters containing both colloidal sizes was observed for both 100 : 50 and 50 : 25 nm combinations (Fig. S3, ESI†), suggesting that the distribution of

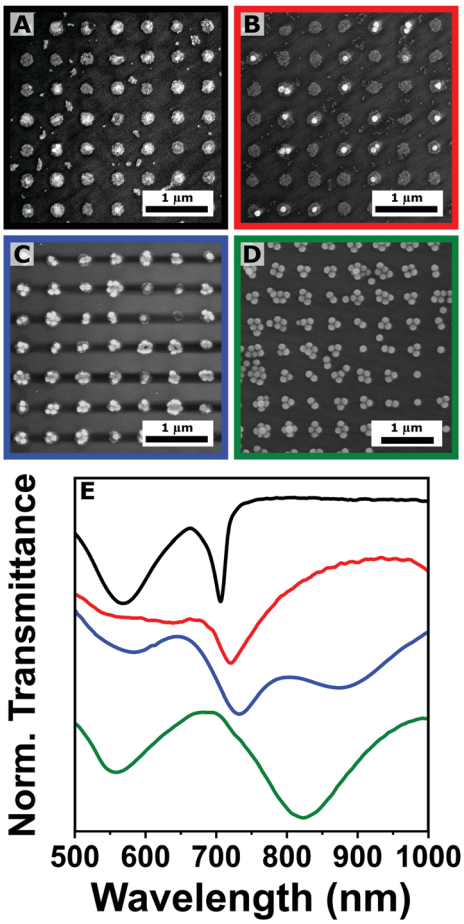

Fig. 2 (A)–(D) Scanning electron microscopy analysis of plasmonic arrays (Λ = 500 nm) fabricated by co-assembling of gold nanoparticles of 25 and 100 nm in diameter. The volume fraction of the 25 nm colloid is 1 (A), 0.5 (B), 0.25 (C), and 0 (D), respectively. (E) Corresponding transmittance spectra with the same color code: volume fraction of 25 nm colloids equal to 1 (black), 0.5 (red), 0.3 (blue), and 0 (green). The spectra were stacked for clarity. Additional SEM images at different magnifications can be found in Fig. S5 in the ESI.†

the two populations of nanoparticles is strongly related to the difference between their translational diffusion coefficients. Another important effect can be observed in the internal organization of each cluster. In the case of homogeneous colloidal distributions, nanoparticles tend to form hexagonal Close-Packed (hpc) supercrystals as the most thermodynamically favorable structure.[25,30] In the case of bimodal size distribution, this internal organization is affected, and the formed clusters do not present a clear internal organization.

Transmittance was measured for all the assemblies with a clear trend observed in their collective response. In fact, while the LPR appears as a sharp peak at 750 nm for the 25 nm colloid (in accordance with eqn (1)), it progressively red shifts and broadens when the fraction of the bigger 100 nm colloid increases (Fig. 2(E)). Both behaviors (the broadening and the bathochromic shift) can be explained by the intensification of the optical losses of the system created by the near-field coupling involving bigger colloids, as demonstrated theoretically by Manjavacas and co-workers.[10] Despite the augmented losses in the repeating unit cell, the emergence of a collective plasmonic response is evident for all the tested mixtures, suggesting the possibility of self-assembling colloids that are significantly different in size (and/or shape). This versatility and resilience of the procedure can be exploited for engineering near- and far-field response of the assembled system, targeting complex architectures where different nanoparticles (*e.g.* magnetic, dielectric or semiconducting nanoparticles) are assembled into hierarchical structures, a key advantage for several applications. Similar structures were recently achieved by Xing *et al.*[37] However, their approach involves several lithographic and metal evaporation steps, instead of relying entirely on colloidal nanoparticles. A promising alternative in this direction could be the implementation of a multistep assembly approach, where the low-diffusion component is preloaded into the PDMS mold, and subsequently transferred to the substrate and simultaneously co-assembled with the high-diffusion component (this approach is discussed further in the ESI,† Fig. S4).

2.2 Pre-assembly modifications: the effect of colloid composition

Another sensible approach for changing the plasmonic properties of the arrays is to alter the composition of the repeating units. In our second study, we combined gold and silver nanoparticles of 49 ± 3 and 45 ± 4 nm respectively (Fig. S1, ESI†), varying the Au : Ag proportion of the mixture before self-assembly. The choice of silver is motivated by its better plasmonic performance with respect to gold. Specifically, we prepared four colloidal suspensions with a volume fraction of gold nanoparticles (ϕ_{Au}) of 1 (pure gold), 0.75, 0.35 and 0 (pure silver). The mixtures were characterized by UV-vis spectroscopy and the composition was confirmed by energy dispersive X-ray (EDX) spectroscopy (Fig. S2, ESI†).

The successful preparation of plasmonic arrays was confirmed by SEM analysis (Fig. 3(A)–(D)). Taking advantage of the different electronic contrast between the two elements, gold and silver particles can be identified in the bright-field images, similar to what is commonly observed for bimetallic structures,[38] and showing a statistical distribution of the two colloids within the different clusters. This was expected, as both gold and silver nanoparticles have similar sizes, have the same coating, and are dispersed in the same medium. The different composition of the four colloidal suspensions was reflected in the transmission spectra of the prepared assemblies (Fig. 3(E)). In the 400–700 nm region, the LSPRs associated with the clusters highlight the emergence of resonances in the blue region of the spectra as the fraction of silver colloid is increased, compared to the more red shifted the localized plasmons associated to gold nanoaprticles (>600 nm). Moreover, the optical characterization confirms the emergence of a lattice plasmon resonance centered around 750 nm for all the samples (Fig. 3(E)), once again in accordance with the prediction of eqn (1). The characteristic angular dependence of the LPR peaks was also analyzed by varying the illumination angle (Fig. S6, ESI†). Under normal incidence, two trends can

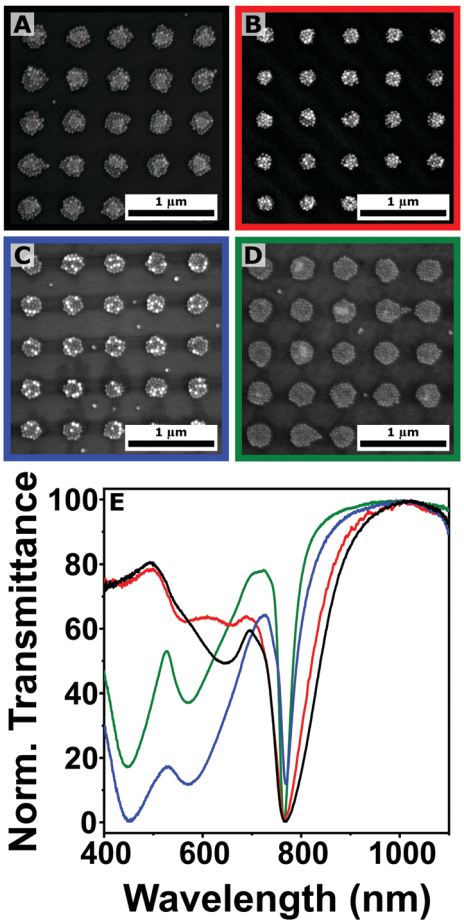

Fig. 3 (A)–(D) Scanning electron microscopy analysis of plasmonic arrays (Λ = 500 nm) fabricated by co-assembling of gold and silver nanoparticles of ~50 nm in diameter. The volume fraction of the gold colloid (ϕ_{Au}) is 1 (A), 0.75 (B), 0.35 (C), and 0 (D), respectively. (E) The corresponding normalized transmittance spectra following the same color code: volume fraction of gold colloids equal to 1 (black), 0.75 (red), 0.35 (blue), and 0 (green). Additional SEM images at different magnifications can be found in Fig. S8 in the ESI.†

be clearly observed (Fig. 3(E)). The first is a progressive red shift in the spectral position of the LPRs, going from gold (770 nm) to silver (765 nm). However, this cannot be considered significant, as sample to sample variation can cause similar shifts in the position of the lattice resonances (Fig. S7, ESI†), probably due to a slight variation in n_{eff} or to a not completely uniform distribution of the colloid upon solvent evaporation. The second effect consists of an improvement in the quality factors (Q_F) of the LPRs as the fraction of silver is increased, going from Q_F of 6 to 7, 15, and 25, due to the higher plasmonic performance of silver. This increment demonstrates how different compositions affect the collective plasmonic properties of the array. This effect can be engineered further in post-assembly modificiations of the plasmonic arrays.

2.3 Post-assembly modifications: thermal annealing

Another possibility to tune the collective plasmonic properties of the array is to modify the internal structure of the repeating units once the self-assembly step is already completed. The use of thermal annealing steps to improve the crystallinity of evaporated films is quite common for top-down lithographic approaches.[39] Taking inspiration from this type of treatments, the same plasmonic arrays analyzed in Fig. 3 were heated using a rapid thermal annealing (RTA) system under nitrogen atmosphere and a mild vacuum (10^{-2} torr). The nanometric size of the colloids enabled the use of lower annealing temperatures compared to standard methodologies, which can involve thermal steps as high as 900 °C.[40] Specifically, two different temperatures were selected for this study: 300, and 450 °C, with an equal dwelling time of 60 min.[41]

During the annealing procedure, two different effects have to be taken into consideration. The first is the elimination of the organic ligand surrounding (and stabilizing) the individual nanoparticles composing the clusters. By thermally decomposing the coating shell, the surface energy of the nanoparticles will increase, allowing the more energized surface atoms to rearrange even below the nanoparticle melting point.[41–43] This effect combined with the short interparticle distance inside the clusters (<2 nm), induces the coalescence of the 50 nm colloids into a single plasmonic unit. This would eliminate the near-field coupling existing within the clusters, reducing the optical losses within the system and yielding sharper LPRs. The second process that needs to be evaluated is the internal migration of atoms within the formed structure, which is particularly interesting in the case of heterogeneous cluster composition, as in the case of gold and silver nanoparticles presented in Fig. 3. According to *in situ* studies performed recently on bimetallic systems by advanced electron microscopy,[44–46] at 450 °C it should be possible to achieve complete alloying of the two metals, while at lower temperature the atom migration should be prevented or considerably slower.

We started by analyzing the effect of the thermal annealing on plasmonic arrays composed by solely gold or silver nanoparticles (Fig. 4). Bright-field SEM analysis confirms the modification of the clusters after annealing; however, there are important differences between the two metals. In the case of gold, a single almost isotropic shape was obtained at both annealing temperatures (Fig. 4(A), (C) and (E)). A slight reduction in size is expected, as the heated particles tend to dewet from the surface.[47–49] On the contrary, clusters composed of silver spheres do not completely merge, yielding irregular and inhomogeneous structures composed of few sintered nanoparticles (Fig. 4(B), (D) and (F)). This behavior is reflected a much smaller size reduction of the clusters (Fig. S13, ESI†), and cannot be explained by a difference in the melting points, which is lower in the case of 50 nm silver nanoparticles (1064 *vs.* 962 °C for gold and silver, respectively).[50,51] Similarly, oxidation of the silver colloids seems unlikely, as the entire annealing procedure is performed under nitrogen atmosphere and vacuum conditions; consequently, the oxygen partial pressure should not be enough to promote oxygen adsorption over the particles.[52] The observed different behavior could instead be attributed to two (possibly coexisting) effects. The first one is the formation of silver sulfide species following the degradation of the coating PEG-SH ligands.[53] The second

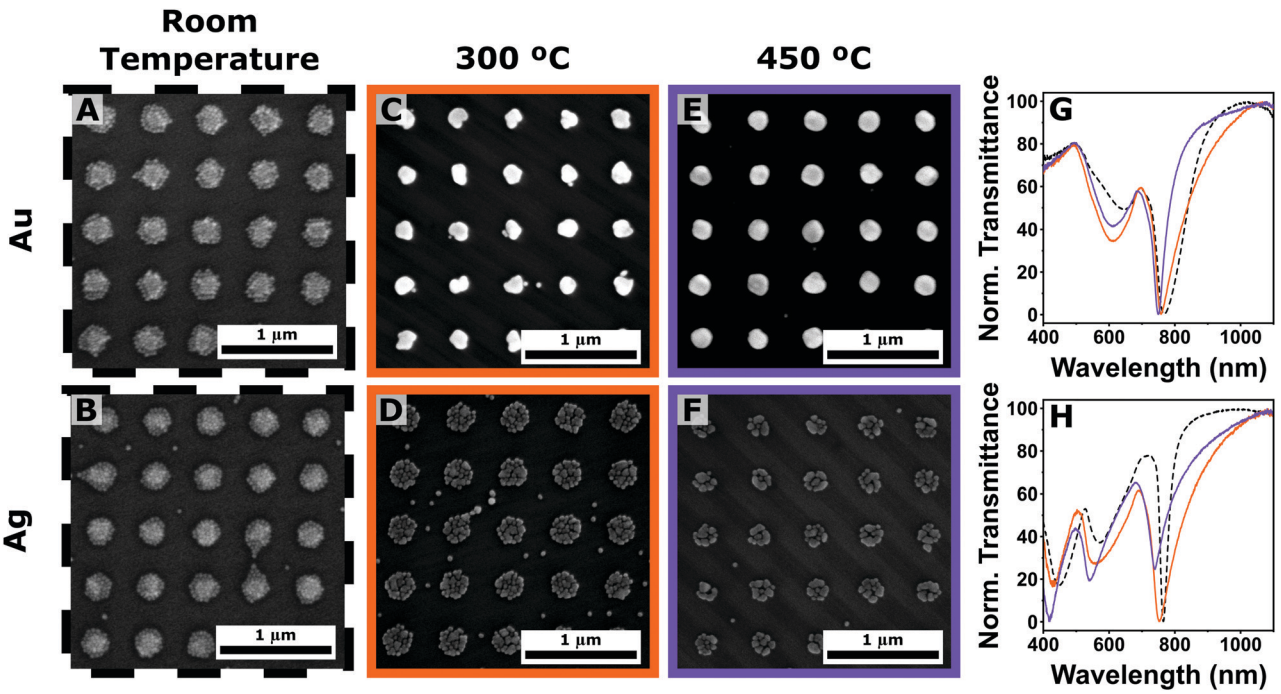

Fig. 4 (A)–(F) Scanning electron microscopy (SEM) analysis of plasmonic arrays (Λ = 500 nm) composed of gold (top row) and silver (bottom row) nanoparticles at room temperature (A), (B), and subjected to thermal annealing at 300 (C), (D) and 450 °C (E), (F). (G) and (H) Corresponding transmittance spectra with the same color code: room temperature (dotted black lines), annealing temperatures of 300 (purple solid lines), and 450 °C (orange solid lines) in the case of gold (G) and silver (H). Additional SEM images and the illumination angle dependency can be found in Fig. S9 and S10 in the ESI,† respectively.

effect concerns the tendency of gold and silver particles to coalesce, which is directly related to different surface atom mobility,[46] associated with surface energy, cohesive energy and vacancy formation.[54] The dewetting of silver and gold upon annealing of evaporated thin films has been used for the preparation of metallic islands, and it has been shown to depend upon several factors, including pressure, atmosphere composition, wettability of the surface, annealing temperature and heating ramp, as well as thickness and crystallinity of the film.[55–59] These effects were recently studied by Bronchy *et al.* for the sintering of silver nanocubes.[41] In this study, we decided to maintain the RTA profile consistent for all the samples, in order to identify potential advantages in the use of mixture colloids for the preparation of annealed plasmonic arrays.

The difference in morphology is reflected in the resulting optical responses of the arrays (Fig. 4(G) and (H)). In the case of gold colloid, a significant reduction of the LPR bandwidth was observed (Q_F of 6, 11, and 16 for RT, 300 and 450 °C respectively, Fig. 4(G)). On the contrary, silver plasmonic arrays registered a broadening and intensity reduction of the LPR peaks leading to a worsening of the Q factors (Q_F of 25, 10, and 12 for RT, 300 and 450 °C respectively, Fig. 4(H)), suggesting the emergence of more optical losses in the system, or a reduction in the far-field coupling amongst the repeating units.

The analysis of the annealing step was extended to the plasmonic arrays prepared by the two mixtures of gold and silver colloids (Fig. 5). Interestingly, the presence of gold within the clusters seems to facilitate the merging of the colloids into single structures, even when it is the minority component of the mixture (Fig. 5(A)–(D)).

Apart from bright-field characterization, EDX mapping (red trace for gold and green trace for silver) was performed on the obtained structures for both annealing temperatures (Fig. 5(E)–(H)). At 300 °C, the elemental analysis showed the formation of heterogeneous areas within the same plasmonic unit cells for both mixtures (Fig. 5(E) and (F)). These results suggest the possibility to control the formation of patchy structures where the location of the different elements could be engineered during the assembly, with great potential for plasmonic-driven (photo)catalysis, where the energy or electron transfer between the plasmonic unit and the catalytic site has to be carefully designed. When the annealing temperature was increased to 450 °C, the spatial distribution of gold and silver recorded by EDX mapping analysis shows a substantially different scenario, with the two elements completely overlapping, pointing towards the formation of alloyed structures (Fig. 5(G) and (H)). The effect of a higher annealing temperature is also reflected in the reduction of the cluster size (Fig. S13, ESI†). Metal alloying represents a resourceful direction for engineering the dielectric constant of a material, which could have significant implication for the plasmonic properties of the system.[60] Indeed, our fabrication scheme can be extended to any other composition, targeting the desired alloy depending on the specific property or application of interest.

The analysis of the transmittance profiles shows similar trends as the one shown in Fig. 4: the Q_F associated with the LPRs is

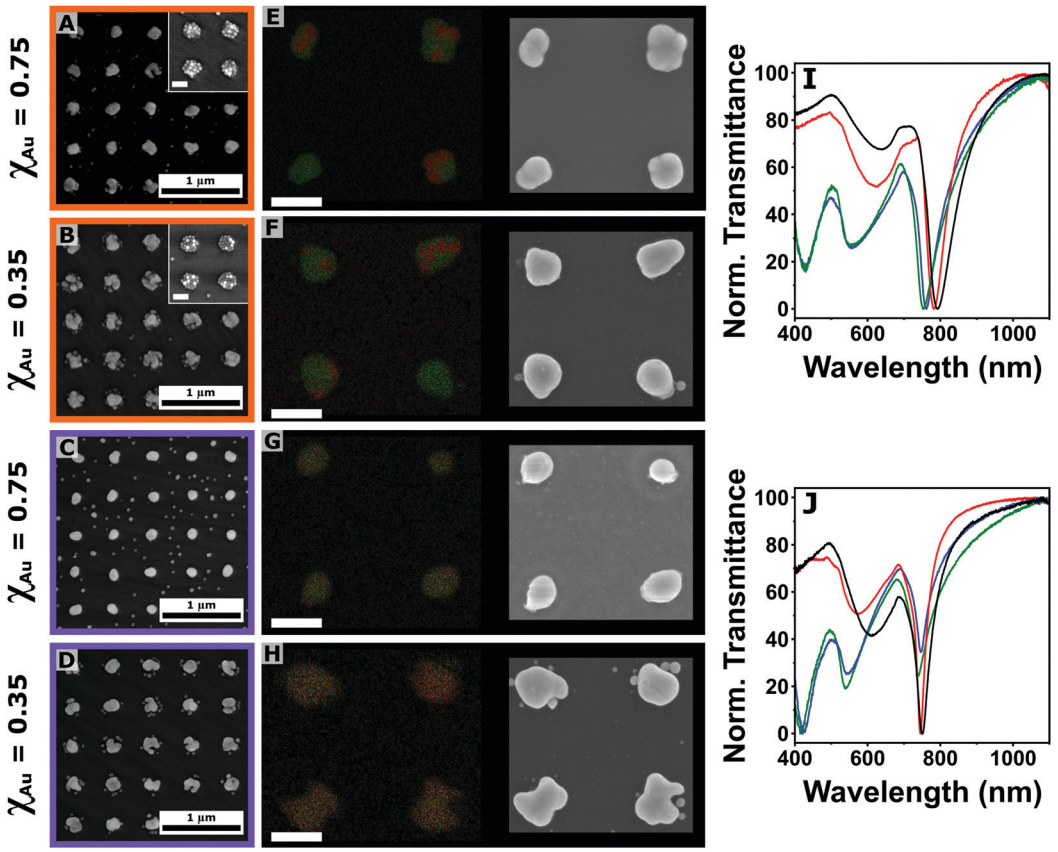

Fig. 5 (A)–(D) Scanning electron microscopy (SEM) analysis of plasmonic arrays (Λ = 500 nm) composed of a mixture of gold and silver colloids with ϕ_{Au} = 0.75 (A), (C), and 0.35 (B), (D) subjected to thermal annealing at 300 (A), (B) and 450 °C (C), (D). The inset in A and B show the clusters at room temperature (scale bar: 200 nm). (E)–(H) Energy dispersive X-ray spectroscopy mapping of the plasmonic arrays (Λ = 500 nm) composed of a mixture of gold (red trace) and silver (green trace) colloids with ϕ_{Au} = 0.75 (E), (G), and 0.35 (F), (H) subjected to thermal annealing at 300 (E), (F) and 450 °C (G), (H). On the right side the corresponding bright-field images. Scale bar: 200 nm. (I) and (J) Normalized transmittance spectra of plasmonic arrays after thermal annealing at 300 (I) and 450 °C (J) as a function of the gold molar fraction (ϕ_{Au}): 1 (pure gold, black line), 0.75 (red line), 0.35 (blue line) and 0 (pure silver, green line). Additional SEM images and the illumination angle dependency can be found in Fig. S11 and S12 in the ESI.†

increased with the annealing temperature when gold is the main component of the initial colloidal mixture, while it decreases for the silver-rich arrays. Another important observation is that for both annealing temperatures, the best optical performance is reached by the ϕ_{Au} = 0.75 sample (Fig. 5(I) and (J)). This shows how the combination of gold and silver could improve the optical performance of a colloidal nanoparticle array combining the optical performance of silver and the chemical and physical stability of gold. Specifically, a Q_F of 20 was recorded for the corresponding LPR after 450 °C annealing, the second highest reported in this study after the one obtained for pure silver arrays (Q_F = 24), representing an increment of ~20% for a monometallic gold array annealed at the same temperature.

3. Conclusions

In conclusion, we investigated the effect of both pre- and post-assembly modifications of the repeating unit of plasmonic arrays on the structural and optical properties of the system. This work demonstrates the versatility of the templated self-assembly approach for the use of multiple components for the preparation of plasmonic arrays with a higher degree of complexity. The integration of multiple components with significantly different size and composition does not disrupt the assembly process, pointing towards the opportunity of creating arrays of hierarchical structures that could open the door to sophisticated photonic architectures combining plasmonic, semiconducting, and dielectric colloids. In the absence of preferential interactions, gold and silver colloids followed a statistical distribution within the array, but an interesting future direction could be to leverage directional and specific interparticle interactions in order to achieve a higher level of control over the colloidal organization within the single repeating unit. This new level of engineering could be exploited even further by post-assembly modifications. In this work, a mild thermal annealing step was used to fabricate heterogeneous patchy structures or alloys by simply varying the annealing temperature between 300 and 450 °C. This approach holds incredible potential for the preparation of plasmonic structures that could not be targeted by standard top-down lithographic methods, and for the preparation of alloyed structures particularly suitable for specific applications.

For example, the integration of catalytic metals such as palladium or platinum into this preparation scheme could be particularly interesting for plasmon-based (photo)catalysis and optoelectronics devices.

Author contributions

The experiments were designed by L. S., O. C. F., S. T. C. and Y. C; Y. C., O. C. F. and S. T. C. led the colloidal and self-assembly optimization; D. M. Q., L. S. and Y. C. led the optimization of the thermal annealing step. Data were collected by O. C. F., S. T. C., Y. C., and L. S. Figures were prepared by O. C. F., S. T. C., and L. S. The manuscript was written by L. S., and A. M. with assistance from all other authors. All authors have given approval to the final version of the manuscript.

Conflicts of interest

There are no conflicts to declare.

Acknowledgements

The authors would like to thank Marta Gerbolés Gibert and the Nanoquim cleanroom facility at the Institute of Materials science of Barcelona (ICMAB-CSIC) for their support with the rapid thermal annealing experiments and Marcos Rosado Iglesias for the assistance during the advanced electron microscopy and energy dispersive X-ray spectroscopy measurements conducted at the Catalan Institute of Nanoscience and Nanotechnology (ICN2). This project had received funding from the Spanish Ministerio de Ciencia e Innovación through grant, PID2019-106860GB-I00 and FUNFUTURE (CEX2019-000917-S), in the framework of the Spanish Severo Ochoa Centre of Excellence program. L. S. and Y. C. research is supported by the 2020 Post-doctoral Junior Leader-Incoming Fellowship by ''la Caixa'' Foundation (ID 100010434, fellow-ship code LCF/BQ/PI20/11760028). O. C. F. was supported by a JAE-INTRO fellowship from the Spanish Ministerio de Ciencia e Innovación (JAEINT21_EX0577). Y. C. acknowledges financial support from the UAB under the auspices of the UAB material science doctoral program.

Notes and references

1 S. A. Maier, *Plasmonics: Fundamentals and Applications*, Springer, vol. 1, 2007.
2 S. E. Lohse and C. J. Murphy, *J. Am. Chem. Soc.*, 2012, **134**, 15607–15620.
3 D. J. de Aberasturi, A. B. Serrano-Montes and L. M. Liz-Marzán, *Adv. Opt. Mater.*, 2015, **3**, 602–617.
4 V. G. Kravets, A. V. Kabashin, W. L. Barnes and A. N. Grigorenko, *Chem. Rev.*, 2018, **118**, 5912–5951.
5 L. Scarabelli, *Pure Appl. Chem.*, 2018, **90**, 1393–1407.
6 C. Cherqui, M. R. Bourgeois, D. Wang and G. C. Schatz, *Acc. Chem. Res.*, 2019, **52**, 2548–2558.
7 W. Wang, M. Ramezani, A. I. Väkeväinen, P. Törmä, J. G. Rivas and T. W. Odom, *Mater. Today*, 2018, **21**, 303–314.
8 A. A. Darweesh, S. J. Bauman, D. T. Debu and J. B. Herzog, *Nanomaterials*, 2018, **8**, 809.
9 V. G. Kravets, F. Schedin and A. N. Grigorenko, *Phys. Rev. Lett.*, 2008, **101**, 087403.
10 A. Manjavacas, L. Zundel and S. Sanders, *ACS Nano.*, 2019, **13**, 10682–10693.
11 S. Baur, S. Sanders and A. Manjavacas, *ACS Nano.*, 2018, **12**, 1618–1629.
12 E. Ponomareva, K. Volk, P. Mulvaney and M. Karg, *Langmuir*, 2020, **36**, 13601–13612.
13 M. Tebbe, M. Mayer, B. A. Glatz, C. Hanske, P. T. Probst, M. B. Müller, M. Karg, M. Chanana, T. A. F. König and C. Kuttner, *et al.*, *Faraday Discuss.*, 2015, **181**, 243–260.
14 M. Juodėnas, T. Tamulevičius, J. Henzie, D. Erts and S. Tamulevičius, *ACS Nano.*, 2019, **13**, 9038–9047.
15 Q.-Y. Lin, J. A. Mason, Z. Li, W. Zhou, M. N. O'Brien, K. A. Brown, M. R. Jones, S. Butun, B. Lee and V. P. Dravid, *et al.*, *Science*, 2018, **359**, 669–672.
16 H. Zhang, C. Kinnear and P. Mulvaney, *Adv. Mater.*, 2020, **32**, 1904551.
17 H. Zhang, J. Cadusch, C. Kinnear, T. James, A. Roberts and P. Mulvaney, *ACS Nano.*, 2018, **12**, 7529–7537.
18 J. B. Lee, H. Walker, Y. Li, T. W. Nam, A. Rakovich, R. Sapienza, Y. S. Jung, Y. S. Nam, S. A. Maier and E. Cortés, *ACS Nano.*, 2020, **14**, 17693–17703.
19 L. Scarabelli, D. Vila-Liarte, A. Mihi and L. M. Liz-Marzán, *Acc. Mater. Res.*, 2021, **2**, 816–827.
20 D. Vila-Liarte, M. W. Feil, A. Manzi, J. L. Garcia-Pomar, H. Huang, M. Döblinger, L. M. Liz-Marzán, J. Feldmann, L. Polavarapu and A. Mihi, *Angew. Chem., Int. Ed.*, 2020, **59**, 17750–17756.
21 V. Lotito and T. Zambelli, *Adv. Colloid Interface Sci.*, 2022, **299**, 102538.
22 Y. Brasse, V. Gupta, H. C. T. Schollbach, M. Karg, T. A. F. König and A. Fery, *Adv. Mater. Interfaces*, 2020, **7**, 1901678.
23 P. T. Probst, M. Mayer, V. Gupta, A. M. Steiner, Z. Zhou, G. K. Auernhammer, T. A. F. König and A. Fery, *Nat. Mater.*, 2021, 1–5.
24 N. J. Greybush, M. Saboktakin, X. Ye, C. Della Giovampaola, S. J. Oh, N. E. Berry, N. Engheta, C. B. Murray and C. R. Kagan, *ACS Nano.*, 2014, **8**, 9482–9491.
25 C. Matricardi, C. Hanske, J. L. Garcia-Pomar, J. Langer, A. Mihi and L. M. Liz-Marzán, *ACS Nano.*, 2018, **12**, 8531–8539.
26 J. Plou, M. Charconnet, I. García, J. Calvo and L. M. Liz-Marzan, *ACS Nano.*, 2021, **15**, 8984–8995.
27 J. Plou, I. García, M. Charconnet, I. Astobiza, C. García-Astrain, C. Matricardi, A. Mihi, A. Carracedo and L. M. Liz-Marzán, *Adv. Funct. Mater.*, 2020, **30**, 1910335.
28 M. Torras, P. Molet, L. Soler, J. Llorca, A. Roig and A. Mihi, *Adv. Energy Mater.*, 2022, **12**, 2103733.
29 C. Hamon, M. N. Sanz-Ortiz, E. Modin, E. H. Hill, L. Scarabelli, A. Chuvilin and L. M. Liz-Marzán, *Nanoscale*, 2016, **8**, 7914–7922.
30 P. Molet, N. Passarelli, L. A. Pérez, L. Scarabelli and A. Mihi, *Adv. Opt. Mater.*, 2021, **9**, 2100761.

31 N. G. Bastús, F. Merkoçi, J. Piella and V. Puntes, *Chem. Mater.*, 2014, **26**, 2836–2846.
32 C. Hanske, E. H. Hill, D. Vila-Liarte, G. González-Rubio, C. Matricardi, A. Mihi and L. M. Liz-Marzán, *ACS Appl. Mater. Interfaces*, 2019, **11**, 11763–11771.
33 L. Novotny and B. Hecht, *Principles of Nano-Optics*, Cambridge University Press, Cambridge, 2006.
34 B. Auguié, X. M. Bendaña, W. L. Barnes and F. J. García de Abajo, *Phys. Rev. B: Condens. Matter Mater. Phys.*, 2010, **82**, 155447.
35 D. Khlopin, F. Laux, W. P. Wardley, J. Martin, G. A. Wurtz, J. Plain, N. Bonod, A. V. Zayats, W. Dickson and D. Gérard, *J. Opt. Soc. Am. B*, 2017, **34**, 691–700.
36 L. Scarabelli, A. Sánchez-Iglesias, J. Pérez-Juste and L. M. Liz-Marzán, *J. Phys. Chem. Lett.*, 2015, **6**, 4270–4279.
37 C. Xing, D. Liu, J. Chen, Y. Fan, F. Zhou, K. Kaur, W. Cai and Y. Li, *Chem. Mater.*, 2021, **33**, 310–319.
38 M. Mayer, L. Scarabelli, K. March, T. Altantzis, M. Tebbe, M. Kociak, S. Bals, F. J. García de Abajo, A. Fery and L. M. Liz-Marzán, *Nano Lett.*, 2015, **15**, 5427–5437.
39 S. Deng, R. Li, J.-E. Park, J. Guan, P. Choo, J. Hu, P. J. M. Smeets and T. W. Odom, *Proc. Natl. Acad. Sci. U. S. A.*, 2020, **117**, 23380–23384.
40 M. Higashino, S. Murai and K. Tanaka, *J. Phys. Chem. C*, 2020, **124**, 27687–27693.
41 M. Bronchy, L. Roach, L. Mendizabal, C. Feautrier, E. Durand, J.-M. Heintz, E. Duguet and M. Tréguer-Delapierre, *J. Phys. Chem. C*, 2022, **126**, 1644–1650.
42 S. Inasawa, M. Sugiyama and Y. Yamaguchi, *J. Phys. Chem. B*, 2005, **109**, 3104–3111.
43 S. K. Cha, J. H. Mun, T. Chang, S. Y. Kim, J. Y. Kim, H. M. Jin, J. Y. Lee, J. Shin, K. H. Kim and S. O. Kim, *ACS Nano.*, 2015, **9**, 5536–5543.
44 A. Skorikov, W. Albrecht, E. Bladt, X. Xie, J. E. S. van der Hoeven, A. van Blaaderen, S. Van Aert and S. Bals, *ACS Nano.*, 2019, **13**, 13421–13429.
45 M. Mychinko, A. Skorikov, W. Albrecht, A. Sánchez-Iglesias, X. Zhuo, V. Kumar, L. M. Liz-Marzán and S. Bals, *Small*, 2021, **17**, 2102348.
46 J. E. S. van der Hoeven, T. A. J. Welling, T. A. G. Silva, J. E. van den Reijen, C. La Fontaine, X. Carrier, C. Louis, A. van Blaaderen and P. E. de Jongh, *ACS Nano.*, 2018, **12**, 8467–8476.
47 C. L. Haynes and R. P. Van Duyne, *J. Phys. Chem. B*, 2001, **105**, 5599–5611.
48 B. J. Y. Tan, C. H. Sow, T. S. Koh, K. C. Chin, A. T. S. Wee and C. K. Ong, *J. Phys. Chem. B*, 2005, **109**, 11100–11109.
49 M. Bechelany, X. Maeder, J. Riesterer, J. Hankache, D. Lerose, S. Christiansen, J. Michler and L. Philippe, *Cryst. Growth Des.*, 2010, **10**, 587–596.
50 J. Lee, J. Lee, T. Tanaka and H. Mori, *Nanotechnology*, 2009, **20**, 475706.
51 S. A. Little, T. Begou, R. W. Collins and S. Marsillac, *Appl. Phys. Lett.*, 2012, **100**, 051107.
52 S. Ozawa, K. Morohoshi, T. Hibiya and H. Fukuyama, *J. Appl. Phys.*, 2010, **107**, 014910.
53 C. Battocchio, C. Meneghini, I. Fratoddi, I. Venditti, M. V. Russo, G. Aquilanti, C. Maurizio, F. Bondino, R. Matassa and M. Rossi, *et al.*, *J. Phys. Chem. C*, 2012, **116**, 19571–19578.
54 K. K. Nanda, S. N. Sahu and S. N. Behera, *Phys. Rev. A: At., Mol., Opt. Phys.*, 2002, **66**, 013208.
55 A. Roy, A. Maiti, T. K. Chini and B. Satpati, *ACS Appl. Mater. Interfaces*, 2017, **9**, 34405–34415.
56 C. V. Thompson, *Annu. Rev. Mater. Res.*, 2012, **42**, 399–434.
57 H. Oh, A. Pyatenko and M. Lee, *Appl. Surf. Sci.*, 2021, **542**, 148613.
58 A. Araújo, M. J. Mendes, T. Mateus, A. Vicente, D. Nunes, T. Calmeiro, E. Fortunato, H. Águas and R. Martins, *J. Phys. Chem. C*, 2016, **120**, 18235–18242.
59 K. M. McPeak, S. V. Jayanti, S. J. P. Kress, S. Meyer, S. Iotti, A. Rossinelli and D. J. Norris, *ACS Photonics.*, 2015, **2**, 326–333.
60 C. Gong and M. S. Leite, *ACS Photonics.*, 2016, **3**, 507–513.